

# Microstructure characteristics of spray-formed high speed steel and its evolution during subsequent hot deformation

Lin Lu, Long-gang Hou,<sup>a)</sup> Jin-xiang Zhang, He-bin Wang, Hua Cui, and Jin-feng Huang  
*State Key Laboratory for Advanced Metals and Materials, University of Science and Technology Beijing, Beijing 100083, China*

Yong-an Zhang  
*State Key Laboratory of Non-Ferrous Metals and Process, General Research Institute for Non-Ferrous Metals, Beijing 100088, China*

Ji-Shan Zhang  
*State Key Laboratory for Advanced Metals and Materials, University of Science and Technology Beijing, Beijing 100083, China*

(Received 8 September 2015; accepted 21 December 2015)

The microstructural evolution of spray-formed high speed steel during hot deformation was investigated as well as the effects of spray forming parameters on the porosity formation. Four distinct zones are identified in the as-deposited material, and interstitial porosity is present in the bottom and peripheral zones, while gas-related porosity is mainly found in the central zone. It can keep the porosity at a minimum value by using the optimum parameters, e.g., the average porosity of central zone is 3.7% for a superheat of 170 °C and a gas-to-metal flow rate of 0.7. During hot deformation at 1150 °C, the amount of porosity can be obviously decreased by increasing the height reduction which also plays a key role in breaking up eutectic carbides. The critical height reduction for the breakdown of the eutectic carbides is 50%, the dominant mechanism being mechanical fragmentation.

## I. INTRODUCTION

Spray forming, which was invented by Prof. Singer in the early 80s, has been proved to be an effective method to improve the solidification microstructure of tool steels<sup>1–6</sup> due to the effects of high cooling rate ( $10^3 \sim 10^5$  K/s) during atomization and deformation or fragmentation during deposition.<sup>7,8</sup> It is also widely accepted that the advantages of spray-formed materials are the very fine scale microstructures, fine precipitates, low levels of segregation, extended solid solubility, and presence of metastable phases. One of the main disadvantages of spray-formed materials is the presence of porosity. Although porosity is not always deleterious in spray-formed materials, it is generally undesirable, especially for applications where strength and ductility are critical.

There are lots of studies about the porosity formation<sup>9–12</sup> and the effects of processing parameters on its formation.<sup>13–15</sup> According to these proposed mechanisms of the porosity formation, we could divide the porosity into three categories, such as gas pores, interstitial pores and solidification shrinkage. The gas pores are related to the

presence of an excessive proportion of liquids during deposition. It is reported that for the same material, the gas pores are relatively high when the liquid fraction is high.<sup>11,16</sup> The solidification shrinkage porosity is produced as a result of the large differences in density between the liquid and solid phases.<sup>11</sup> Some studies<sup>17,18</sup> show that a large portion of porosity observed in spray-formed materials may be attributed to interstitial pores. This type of porosity is generally a result of the incomplete filling of the interstices between partially solidified droplets. It is very difficult to distinguish the solidification shrinkage and the gas pores, so the solidification shrinkage is treated as gas pores in this study.

Basing on the deep understanding of the forming mechanisms of porosity, it is now possible to produce spray-formed billets with the density up to 98.5% of theoretical, and some residual porosity is still found.<sup>19</sup> Generally, we can reduce the porosity to the lowest value by optimizing the spray-deposition conditions or by thermo-mechanical processing. Available literature studies mainly focus on improving the density of spray-formed materials by optimizing spray forming parameters. Many reports have used hot isostatic pressing to densify the spray-formed high speed steels, however, the expensive production costs has limited this application. A few studies have been made on the use of hot deformation to improve the microstructures of spray-formed high speed

Contributing Editor: Yang-T Cheng

<sup>a)</sup>Address all correspondence to this author.

e-mail: lghou@skl.ustb.edu.cn

DOI: 10.1557/jmr.2015.407

steels,<sup>19,20</sup> but the effects of hot deformation on microstructure evolution have not been addressed in detail.

This study aims to (i) assess the effects of spray forming process parameters on the porosity formation, (ii) characterize the microstructure evolution during hot deformation, and (iii) determine optimal parameters for hot forging process.

**II. EXPERIMENTAL**

The commercial M2 high speed steel used as the feedstock was melted in a medium-frequency induction furnace, and alloying elements, such as carbon, vanadium, and niobium, were added into the melt at 1550 °C and then atomized. Billets with a diameter of 180 mm and length of 100 mm were prepared using the processing parameters which are shown in Table I. The chemical composition of the experimental steel is: 1.31% C, 6.1% W, 4.9% Mo, 4.48% Cr, 2.75% V, 0.5% Nb, and balance of Fe. The half-cut of the as-deposited billet is shown in Fig. 1(a).

The density was measured using Archimedes’ principle according to GB/T3850-1983, and the theoretical density (8.15 g/cm<sup>3</sup>) was taken to determine the percentage of porosity, on the basis of density measurements, as:

$$p = (1 - \rho_e / \rho_t) \times 100\% \quad , \quad (1)$$

where *p* is the percentage of the porosity, and  $\rho_e$  and  $\rho_t$  is the experimental and theoretical density, respectively.

The hot deformation cylindrical specimens with a diameter of 8 mm and length of 12 mm were cut from the center zone of the billet using wire electrical discharge machining. Hot compression tests were carried out at 1150 °C with a strain rate of 0.1 s<sup>-1</sup> by the Gleeble 1500

TABLE I. Processing parameters of spray forming.

Items	Parameters
Super heat/°C	150–200
Diameter of the delivery tube/mm	4.0
Atomization gas	N <sub>2</sub>
Atomization pressure/MPa	0.4–0.5
Deposition distance/mm	425–450

simulator (Dynamic Systems Inc., St. Paul, Minnesota). All the specimens were heated to 1180 °C with a heating rate of 10 °C/s and soaked for 3 min, and then cooled to 1150 °C with a cooling rate of 3 °C/s. The height reductions are between 20 and 80%.

Microstructural examination was conducted using a field emission scanning electron microscope (SEM). The SEM samples were prepared by grinding and polishing, and etched with 8% nital solution.

**III. RESULTS AND DISCUSSION**

**A. Porosity distribution**

The porosity distribution in the spray-formed M3:2 high speed steel can be classified into four main zones in accordance with the percentage of porosity [Fig. 1(b)], e.g., a bottom band with *p* at a range of 16–42% (red zone), a peripheral zone with an average *p* about 13% (yellow zone), and a surface band with a relatively low porosity about 7% (green zone). The most important zone is the central zone, which has the lowest porosity with the average *p* of 3.7%. In addition, the porosity distribution along the longitudinal [y direction in Fig. 1(b)] and transverse [x direction in Fig. 1(b)] directions is plotted in Fig. 2. It can be seen that the porosity fluctuated slightly as the transverse distance increases when the longitudinal distance is above 20 mm. The curves exhibit inverted “V”-shape at y = 10 mm and y = 20 mm, and the porosity increases continuously until the maximum values at x = 60 mm [Fig. 2(a)]. It is interesting that this point is located at the boundaries of the bottom band and peripheral zone. On the other hand, the porosity along the longitudinal direction shows a sharp decrease, followed by a gradual decrease regardless of the *x* values [Fig. 2(b)]. Various alloy systems exhibit a similar trend of a two stage variation in porosity as a function of deposited thickness,<sup>11</sup> similar to Fig. 1(b). The first stage is associated with the zone close to the substrate where there is a bottom band with the thickness of about 20 mm, in which porosity is relatively high. The mechanisms of porosity formation in this stage are generally attributed to the rapid quench experienced by the droplets that arrive

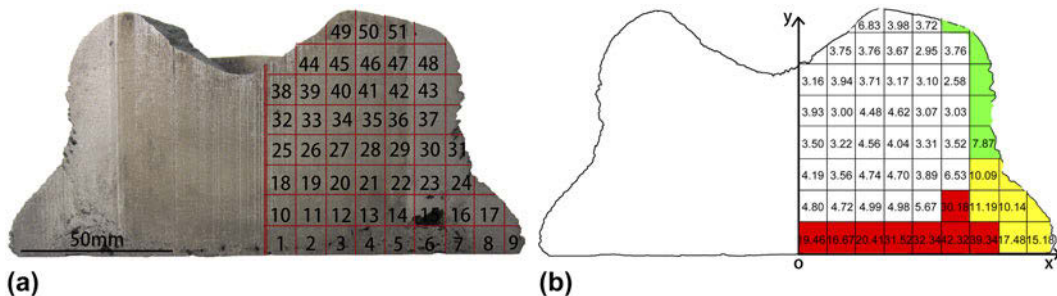


FIG. 1. Half-cut of the as-deposited billet for a melt superheat of 170 °C and a GMR of 0.7: (a) The numbers indicate the sample number for density measurement; (b) Distribution of the porosity corresponds to (a).

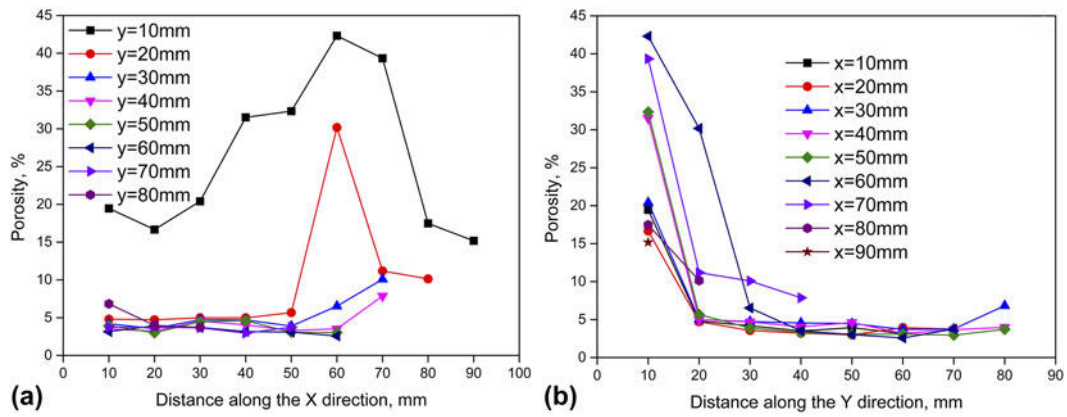


FIG. 2. Distribution of porosity along different directions: (a)  $y$  direction in Fig. 1(b); (b)  $x$  direction in Fig. 1(b).

initially on the cold substrate surface. Therefore, it was reported that the porosity could be decreased in this stage by heating the substrate, reducing the spray distance, or increasing the melt superheat.<sup>21,22</sup> In the second stage, the amount of porosity is insensitive to change in the deposited thickness, and this stage usually corresponds to the steady state conditions in temperature and in mushy layer thickness. The thermal and solidification conditions of the droplets during impact will influence the thickness of mushy layer on the upper surface of the deposit, and, in turn, affect the amount and the morphology of the pores. The relation between the mushy layer and porosity type is illustrated in Ref. 21.

Actually, both the average value of  $p$  and the thickness of each zone are very important, and the latter varies with the spray parameters, such as spray distance and substrate types. For a given spray distance and a steel substrate, the most important parameter, which influences the porosity and the thickness of each zone, is melt superheat. The porosity and thickness of different zones vary with the superheat are shown in Table II. It shows that the porosity and thickness of the bottom zone decrease with increasing melt superheat from 150 °C to 200 °C, however, the porosity in the other three zones decreases and then increases with increasing melt superheat, and the minimum value of porosity is gained at a melt superheat of 170 °C. Moreover, the atomization pressure also has a significant effect on the porosity formation. The values of  $p$  as a function of atomization pressures for a melt superheat of 170 °C are given in Table III. In the central zone, the porosity has the minimum value at an atomization pressure of 0.45 MPa, whereas the value of  $p$  varies monotonically with atomization pressure in the bottom, surface, and periphery zones, e.g.,  $p$  increases from 27.13% to 33.04% as the atomization pressure increases from 0.4 MPa to 0.5 MPa.

### B. Microstructures in different zones

Figure 3 shows the micrograph in the bottom band and peripheral zone. The typical porosity present at the bottom

TABLE II. Thickness and  $p$  of different bands in spray-formed M3:2 high speed steel as a function of melt superheat for an atomization pressure of 0.45 MPa.

Superheat (°C)	Porosity (%)				Thickness (mm)	
	Bottom	Surface	Central	Periphery	Bottom	Surface
150	32.15	8.52	4.63	15.16	13.5	5.5
170	29.03	7	3.7	13	10	5
200	26.74	10.05	4.23	14.79	8.5	4.5

TABLE III. Values of  $p$  in different bands as a function of atomization pressures for a melt superheat of 170 °C.

Atomization pressure (MPa)	Porosity (%)			
	Bottom	Surface	Central	Periphery
0.4	27.13	6.86	4.02	12.07
0.45	29.03	7	3.7	13
0.5	33.04	11.22	3.98	14.89

band is shown in Fig. 3(a), and it is noted that pores in this band have a wide size range between 10 and 500  $\mu\text{m}$  and its volume fraction in the bottom band remained relatively high regardless of the melt superheat and atomization pressure. Most of the large pores have irregular shape while the small ones are nearly spherical. Figure 3(b) shows fine grains with an average size of 25  $\mu\text{m}$  and a great amount of interstitial porosity is located at grain boundaries. Unlike the high porosity and the large-sized pores in the bottom band, the percentage of porosity and the sizes of the pores in the peripheral zone are obviously ameliorated [Fig. 3(c)]. The size of pores in this region are ranged from 5 to 200  $\mu\text{m}$  and some small pores along the layer boundaries are connected together, and leading to large ellipsoidal pores. The microstructures in the peripheral zone have its specific characteristics with respect to the layered structure with pores present at the layer boundaries. It is worth paying attention to that droplets can be discerned in this region, which may experience

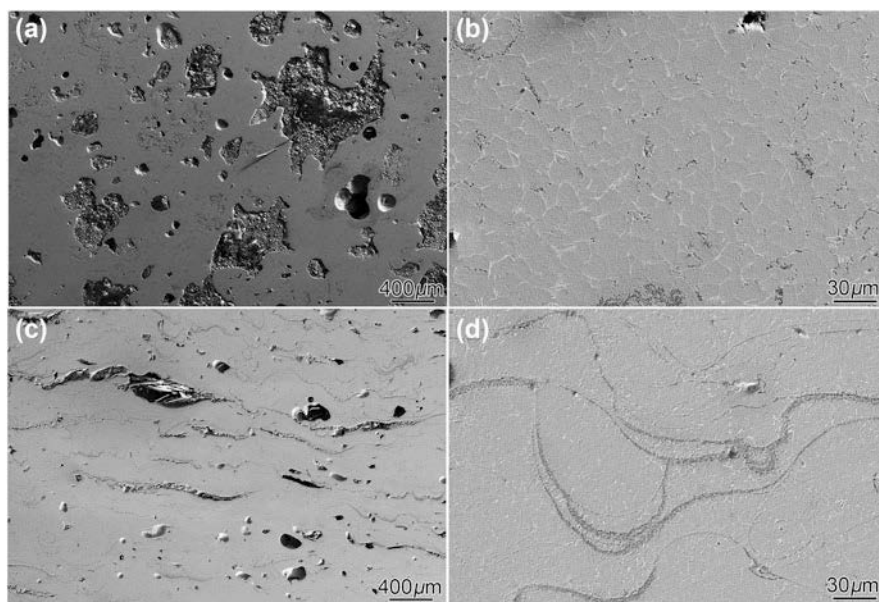


FIG. 3. Microstructures in different zones of as-deposited M3:2 billet: (a) Sample No. 6 in the bottom band; (b) High magnification of (a); (c) Sample No. 9 in peripheral zone; (d) High magnification of (c).

plastic deformation or fracture, and the well-defined boundaries between the deformed droplets observed in Fig. 3(d) suggested that most droplets were in a semisolid or solid state during impingement on the deposited surface. These are typical characteristics of a “cold” spray containing a large proportion of solid phases during impingement.

The microstructure changes in the thickness direction and radial direction of the deposit are shown in Fig. 4. The as-deposited microstructures are consisted of equiaxed grains, discontinuous network of eutectic carbides at the grain boundaries, which has been described in earlier publication.<sup>23</sup> From Figs. 4(a)–4(c), it can be seen that the percentage of the porosity decreases with increasing distance from the deposit bottom to the top, and the types of porosities change from interstitial pores [Fig. 4(a)] into gas pores [Fig. 4(c)] while the pore morphology changes from irregular to spherical. But no apparent changes in grain diameters and the eutectic carbide sizes can be found. For the samples located at 20, 40 and 60 mm from the center of the deposit, there is a small amount of porosity, mainly gas pores [Figs. 4(d)–4(f)]. It shows that the grain diameters and the percentage of porosity decrease with increasing distance from the deposit center to periphery. The average grain size located at 20 mm from the center is 62 μm [Fig. 4(d)] and it decreases to 55 μm [Fig. 4(e)] as the distance increases from 20 to 40 mm, whereas it is 18 μm at 60 mm from center [Fig. 4(f)]. Based on the work of N.H. Prydz,<sup>24</sup> the relationship between local size distribution of the droplets and the radial distance can be expressed as:

$$d_{50}^{\text{local}} = d'_{50} \exp(-r/0.621) \quad , \quad (2)$$

Where  $d'_{50}$  is a constant and  $r$  is radial distances. For Ar and N<sub>2</sub>, the value of  $d'_{50}$  is determined to be 28 and 29 μm, respectively. It is easy to see that local size distribution is characterized by mass median diameter  $d_{50}^{\text{local}}$ , which decreases while moving away from the spray cone centerline. The small droplets cooled quickly than larger ones, and consequently, the grain size decreases as the  $r$  increases. So for the same value of  $r$ , in other words, along the billet thickness direction, no visible changes of the grain size appear [Figs. 4(b) and 4(c)].

### C. Microstructures evolution during hot deformation

Hot deformation is a beneficial process to improve the properties of spray-formed high speed steels since it not only eliminates the porosity but also reconstitutes the microstructure by dynamic recrystallization. The influence of height reduction during hot deformation on the porosity is shown in Fig. 5, and it shows the porosity of all samples decreases about 0.3, 0.6, and 2% with the height reduction of 20, 40, and 70%, respectively. It can be seen that the higher the porosity in the as-deposited microstructure, the higher the porosity in the as-deformed microstructure. This indicates that with a certain height reduction, the porosity of the final deformed samples is determined by the porosity of the original microstructure, and the density of most samples in the central zone can reach 99% of the theoretical value through hot deformation as the height reduction exceeds 80%.

As shown in Fig. 4, the as-deposited structure of M3:2 high speed steel contains lots of eutectic carbides that have a significant influence on the properties. The plate-shaped eutectic carbides have been proved to damage the

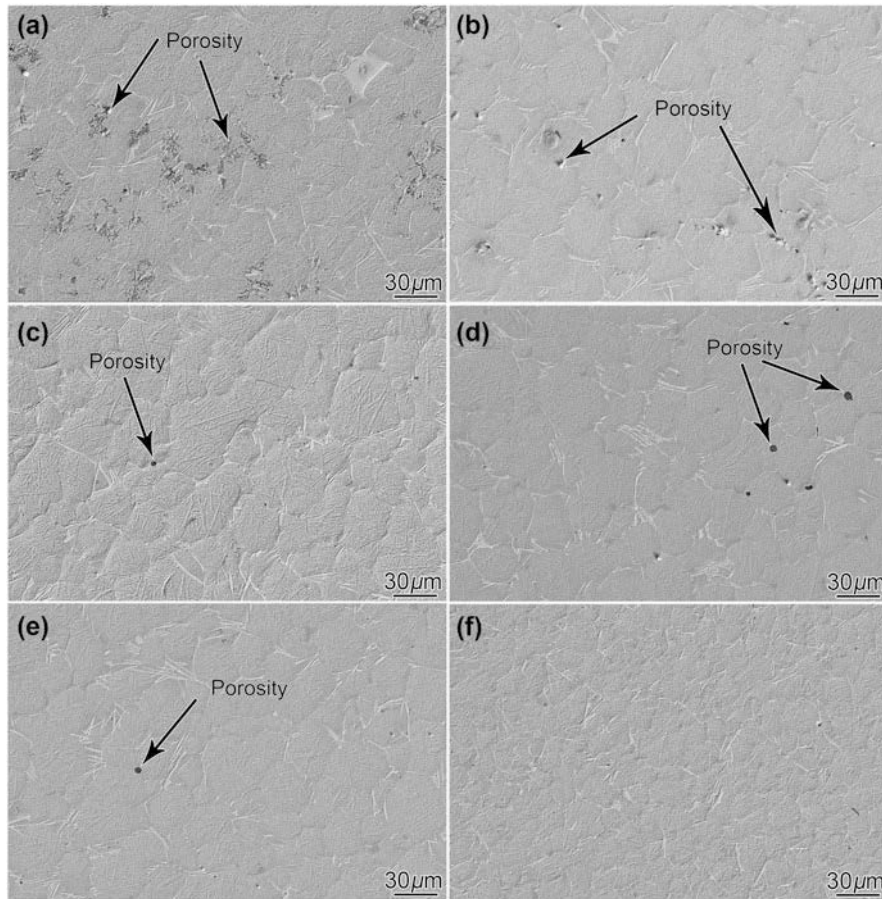


FIG. 4. Secondary electron images of spray-formed M3:2 steel samples from Fig. 1(a): (a) No. 1; (b) No. 18; (c) No. 32; (d) No. 33; (e) No. 35; (f) No. 37.

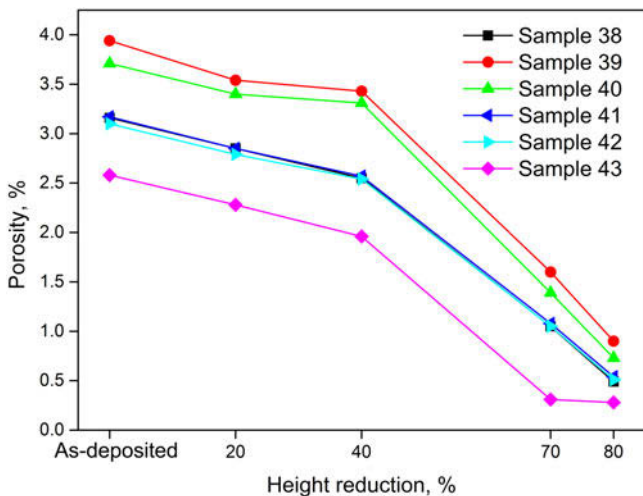


FIG. 5. Effect of height reduction on the porosity of samples in central zone.

bending strength and toughness. Thus the hot deformation mainly aims to improve the size, morphology, and distribution of the carbides. The state of carbides changes remarkably during hot deformation, as shown in Fig. 6. No deformation of the carbide network is observed in

Fig. 6(a). The breakup of  $M_2C$  eutectic carbides is firstly seen in Fig. 6(b) with the height reduction of 40%, although the original eutectic  $M_2C$  carbide colonies are still clearly visible. Further, the eutectic colonies are separated and broken up when the height reduction exceeds 50%, and the carbides are broken into short rod-like and arranged in bands along the normal direction of loading [Fig. 6(c)]. The spheroidization and coarsening of the short rod-like carbides appear under the height reduction of 60% in Fig. 6(d). Once the original eutectic carbides are fragmented into spherical particles and small-sized blocks, their morphologies and sizes are barely changed but dispersed in the matrix with further deformation, as shown in Figs. 6(e) and 6(f). Thus, we can conclude that the critical height reduction for the breakup of plate-like  $M_2C$  carbides and the eutectic colonies are 40 and 50%, respectively. However, it is also worth noting that MC carbides almost remain unchanged, either the morphology or the size. The similar results were found in as-cast M2 high speed steel.<sup>25</sup> Hence, the most effective way to improve the morphology and size of MC carbides is to increase the cooling rate during solidification.

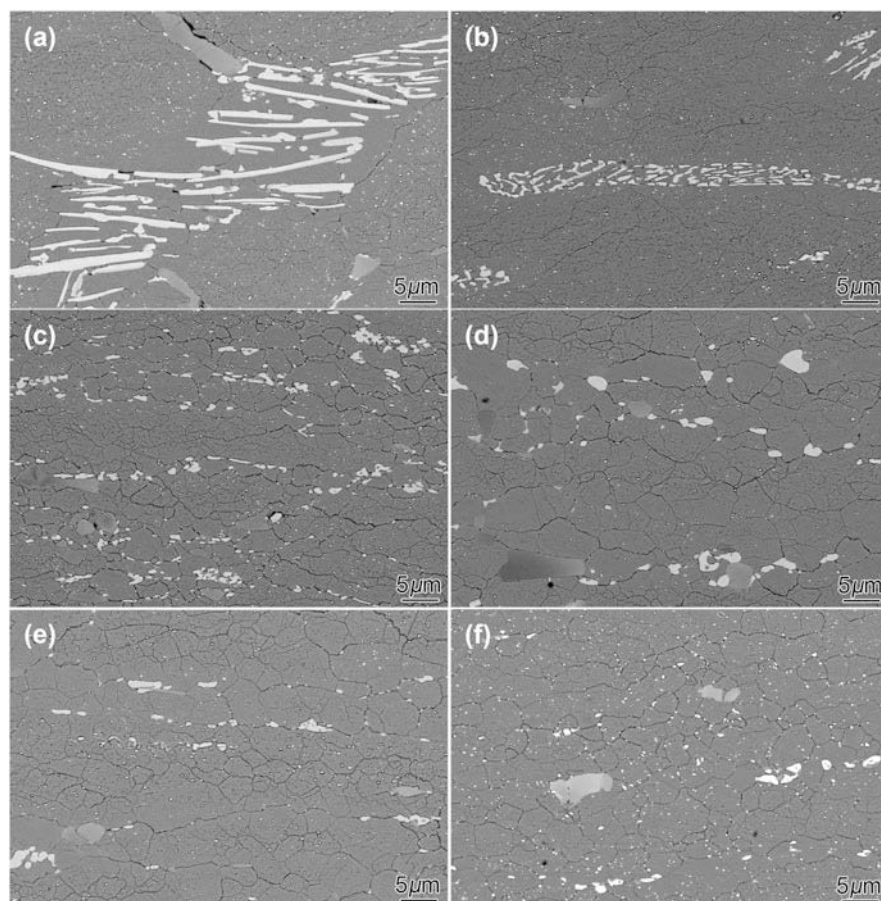


FIG. 6. Back scattered electron images of the as-deformed specimen with different height reductions: (a) 20%; (b) 40%; (c) 50%; (d) 60%; (e) 70%; (f) 80%.

There are two common methods to improve the morphology and size of carbides in steels, e.g., spheroidizing and thermo-mechanical treatment.<sup>25,26</sup> The morphology of carbides changes remarkably during spheroidizing treatment, the process which includes carbide decomposition, dissolution, spheroidization and coarsening. The decomposition and breakup of  $M_2C$  eutectic carbides will occur during hot working process, however, the former occurs mainly during the heating and soaking stage and the latter occurs mainly in deformation stage. For the breakup process, it was shown with the example of M2<sup>25</sup> and M3:2<sup>20</sup> high speed steel that the dominant mechanism for breaking up the eutectic carbide network was mechanical fragmentation as opposed to a diffusion-controlled mechanism. This is supported by this work, where Fig. 6 clearly demonstrates progressive fragmentation by increasing the height reduction. A schematic illustration of carbide evolution during the hot deformation is shown in Fig. 7. When the deformation accumulates to a certain value and the stress difference between the interfaces of carbides and matrix reaches the critical point simultaneously, the carbides cannot deform with the surrounding matrix consistently any more. Consequently, a friction stress,

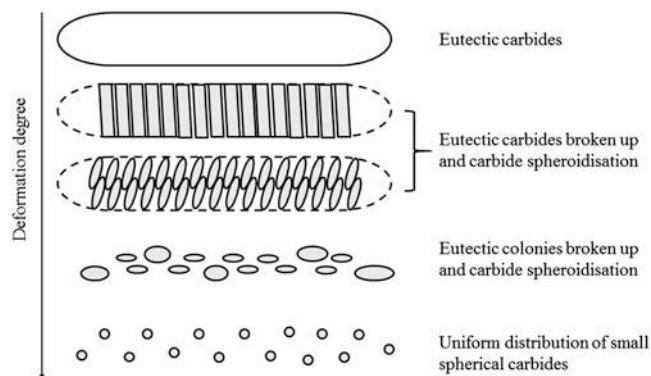


FIG. 7. Schematic of carbide evolution during deformation.

which is responsible for breaking up of carbides, will be produced on the interfaces and if it exceeds the strength of the carbides, the fragmentation of carbides occurs. Presently, the critical height reduction for carbides fragmentation is determined for a single deformation. However, in practice forging of billets, the forging process would be undertaken in progressive smaller strain steps. Nevertheless, the total height reduction allows breakup of carbides.

#### IV. CONCLUSIONS

Microstructure characteristics of spray-formed high speed steel and its evolution during the subsequent hot deformation process are investigated. It shows that the deposition billet can be classified into four main zones: either the bottom band or peripheral zone has a relatively high porosity with mainly irregularly interstitial pores while the lowest porosity is in the central zone ( $p = 3.7\%$ ). The parameters, such as the melt superheat and gas pressure, play an important role in the amount and distribution of the porosity appeared in the deposits, a superheat of 170 °C and a gas-to-metal flow rate (GMR) of 0.7 would be proposed. The density of the deposit can be densified to ~99% theoretical value while the height reduction exceeds 80%, and the critical height reduction for breaking up the plate-like eutectic carbides is 50%.

#### ACKNOWLEDGMENTS

This work was financially supported by the National Basic Research Program of China (No. 2011CB606303) and the Beijing Laboratory of Metallic Materials and Processing for Modern Transportation, China.

#### REFERENCES

1. I.C. Ernst and D. Duh: ESP<sub>4</sub> and TSP<sub>4</sub>, a comparison of spray formed with powdermetallurgically produced cobalt free high-speed steel of type 6W-5Mo-4V-4Cr. *J. Mater. Sci.* **39**, 6831 (2004).
2. I.C. Ernst and D. Duh: Properties of cold-work tool steel X155CrVMo12-1 produced via spray forming and conventional ingot casting. *J. Mater. Sci.* **39**, 6835 (2004).
3. D.N. Hanlon, W.M. Rainforth, C.M. Sellars, R. Price, H.T. Gisborne, and J. Forrest: The structure and properties of spray formed cold rolling mill work roll steels. *J. Mater. Sci.* **33**, 3233 (1998).
4. E.J. Lavernia and N.J. Grant: Spray deposition of metals: A review. *Mater. Sci. Eng.* **98**, 381 (1988).
5. A. Schulz, E. Matthaehi-Schulz, S. Spangel, H. Vettters, and P. Mayr: Analysis of spray formed tool steels. *Materialwiss. Werkstofftech.* **34**, 478 (2003).
6. M. Igharo and J.V. Wood: Investigation of M2 high speed steel produced by Osprey process. *Powder Metall.* **32**, 124 (1989).
7. F. Yan, X. Zhou, H.S. Shi, and J.F. Fan: Microstructure of the spray formed Vanadis 4 steel and its ultrafine structure. *Mater. Charact.* **59**, 592 (2008).
8. P.S. Grant: Solidification in spray forming. *Metall. Mater. Trans. A* **38**, 1520 (2007).
9. B.P. Bewlay and B. Cantor: The relationship between thermal history and microstructure in spray-deposited tin-lead alloys. *J. Mater. Res.* **6**, 1433 (1991).
10. W.D. Cai and E.J. Lavernia: Modeling of porosity during spray forming. *Mater. Sci. Eng., A* **226–228**, 8 (1997).
11. E.J. Lavernia and Y. Wu: *Spray Atomization and Deposition* (John Wiley & Sons, New York, NY, 1996).
12. H.R. Müller, K. Ohla, R. Zauter, and M. Ebner: Effect of reactive elements on porosity in spray-formed copper-alloy Billets. *Mater. Sci. Eng., A* **383**, 78 (2004).
13. W.D. Cai and E.J. Lavernia: Modeling of porosity during spray forming: Part I. Effects of processing parameters. *Metall. Mater. Trans. B* **29**, 1085 (1998).
14. W.D. Cai and E.J. Lavernia: Modeling of porosity during spray forming: Part II. Effects of atomization gas chemistry and alloy compositions. *Metall. Mater. Trans. B* **29**, 1097 (1998).
15. N. Ellendt, O. Stelling, V. Uhlenwinkel, A. von Hehl, and P. Krug: Influence of spray forming process parameters on the microstructure and porosity of Mg<sub>2</sub>Si rich aluminum alloys. *Materialwiss. Werkstofftech.* **41**, 532 (2010).
16. R.H. Bricknell: The structure and properties of a nickel-base superalloy produced by osprey atomization-deposition. *Metall. Trans. A* **17**, 583 (1986).
17. P. Mathur, D. Apelian, and A. Lawley: Analysis of the spray deposition process. *Acta Metall.* **37**, 429 (1989).
18. P.S. Grant, W.T. Kim, and B. Cantor: Spray forming of aluminum-copper alloys. *Mater. Sci. Eng., A* **134**, 1111 (1991).
19. R.A. Mesquita and C.A. Barbosa: Spray forming high speed steel—properties and processing. *Mater. Sci. Eng., A* **383**, 87 (2004).
20. C. Rodenburg, M. Krzyzanowski, J.H. Brynion, and W.M. Rainforth: Hot workability of spray-formed AISI M3:2 high-speed steel. *Mater. Sci. Eng., A* **386**, 420 (2004).
21. H.M. Hu, Z.H. Lee, D.R. White, and E.J. Lavernia: On the evolution of porosity in spray-deposited tool steels. *Metall. Mater. Trans. A* **31**, 725 (2000).
22. S. Spangel, E. Matthaehi-Schulz, A. Schulz, H. Vettters, and P. Mayr: Influence of carbon and chromium content and preform shape on the microstructure of spray formed steel deposits. *Mater. Sci. Eng., A* **326**, 26 (2002).
23. L. Lu, J.F. Huang, L.G. Hou, J.X. Zhang, H.B. Wang, H. Cui, and J.S. Zhang: Effect Of niobium on the microstructure and properties of spray formed M3:2 high speed steel. *J. Univ. Sci. Technol. Beijing* **36**, 1292 (2014).
24. N.H. Pryds, J.H. Hattel, T.B. Pedersen, and J. Thorborg: An integrated numerical model of the spray forming process. *Acta Mater.* **50**, 4075 (2002).
25. M.R. Ghomashchi and C.M. Sellars: Microstructural changes in as-cast M2 grade high speed steel during hot forging. *Metall. Trans. A* **24**, 2171 (1993).
26. M.R. Ghomashchi and C.M. Sellars: Microstructural changes in as-cast M2 grade high speed steel during high temperature treatment. *Met. Sci.* **18**, 44 (1984).